



Microscale Turbulence Measurements Using Doppler Reflectometer and millimeter-wave Scattering System

Tokihiko Tokuzawa^{1,2,3} · Tatsuhiro Nasu² · Daiki Nishimura¹ · Shigeru Inagaki⁴ · Akira Ejiri⁵ · Katsumi Ida^{1,2} · Mikirou Yoshinuma¹ · Tatsuya Kobayashi^{1,2,3} · Kenji Tanaka^{1,3} · Akihide Fujisawa^{1,3} · Ichihiro Yamada¹

Received: 14 July 2025 / Accepted: 22 October 2025 / Published online: 10 November 2025
© The Author(s) 2025

Abstract

To study microscale turbulence, two non-invasive scattering instruments that use electromagnetic waves in the microwave to millimeter-wave range have been installed at the Large Helical Device. One instrument is a Doppler reflectometer, which is suitable for observing turbulence with relatively low wavenumbers. Three circuit systems were constructed for this instrument. The Doppler reflectometer allows a very large number of spatial points (more than 30) to be observed simultaneously in the radial direction and toroidal correlation analysis to be conducted. The other instrument is a two-frequency millimeter-wave scattering system, which was developed to observe turbulence at relatively high wavenumbers. This scattering system has multiple antennas in a vacuum vessel. It can be used to study turbulence anisotropy or, in combination with the Doppler reflectometer, the response of turbulence at various scales.

Keywords Microscale turbulence · Doppler reflectometer · Back-scattering · Frequency comb · Microwave · Millimeter wave

Introduction

A scattering technique that uses electromagnetic waves (e.g., microwaves, millimeter waves, terahertz waves) is suitable for measuring microscale turbulence because such waves do not disturb the plasma and have high temporal and spatial resolutions. When an electromagnetic wave is launched into turbulent plasma, a scattered wave that satisfies the Bragg relationship $k = 2k_i \sin(\theta_s/2)$, where k_i is the local wavenumber of the probing beam and θ_s is the scattering angle, is

generated [1]. Figure 1 shows this Bragg condition for various probe frequencies. The turbulent wavenumber ($k_{\perp} \rho_i$) for an ion gyro radius ρ_i of 0.2 is shown. The figure indicates that either far-forward-scattering or millimeter-wave back-scattering is suitable for observing microscale turbulence. In general, there are two types of scattering, namely collective and non-collective scattering. The scattering parameter (the so-called Salpeter parameter) $\alpha = (k_{\perp} \lambda_{De})^{-1}$ is usually > 1 in typical Large Helical Device (LHD) plasma experiments [2] when the electron density is higher than $1 \times 10^{19} \text{ m}^{-3}$. Here, λ_{De} is the electron Debye length. This means that the scattering is collective and that the scattering signal originates from correlated density fluctuation \tilde{n}_e in scattered power $P_s = \frac{1}{4} r_0^2 |\tilde{n}_e|^2 \lambda_i^2 L^2 P_i$, where r_0 is the classical electron radius, λ_i is the probing wave's wavelength, L is the scattering length, and P_i is the probing wave power [1, 3]. In addition, the probing power of each frequency component is adjusted within a range of several to tens of decibels across the entire system described below.

Considering the installation of a millimeter-wave scattering system at the LHD, appropriate probing frequencies must be selected. The radial profiles of characteristic frequencies for typical LHD plasma parameters (torus major radius location of magnetic axis $R_{ax} = 3.60 \text{ m}$, operational

✉ Tokihiko Tokuzawa
tokuzawa@nifs.ac.jp

¹ National Institute for Fusion Science, National Institutes of Natural Sciences, Toki 509- 5292, Japan

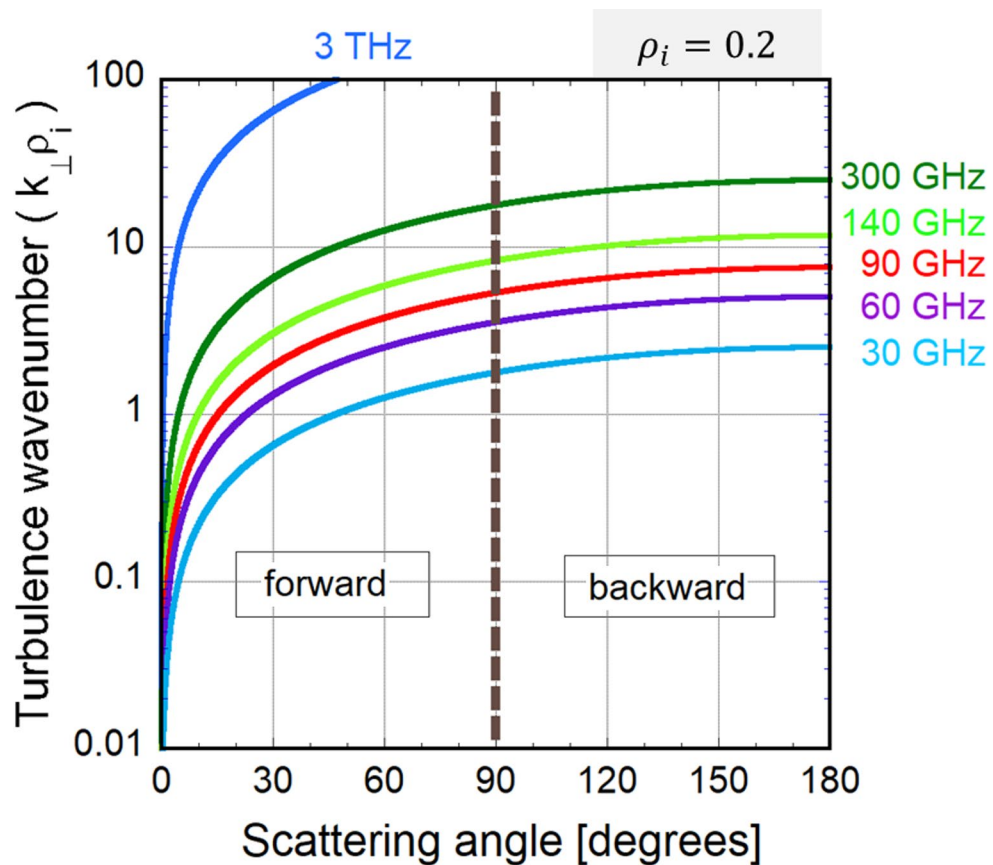
² Department of Fusion Science, The Graduate University for Advanced Study, SOKENDAI, Toki 509-5292, Japan

³ Research Institute for Applied Mechanics, Kyushu University, Kasuga 816-8580, Japan

⁴ Institute of Advanced Energy, Kyoto University, Gokasho 611-0011, Uji, Japan

⁵ Graduate School of Frontier Sciences, The University of Tokyo, Kashiwa 277-8561, Japan

Fig. 1 Bragg relationship between scattering angle and turbulence wavenumber as function of launch frequency. An angle greater than 90° implies back-scattering. The ion gyro radius was calculated to be 0.2



magnetic field strength $B_t = 2.75$ T, $n_e(0) = 4 \times 10^{19}$ m $^{-3}$) are shown in Fig. 2. As shown, the electromagnetic waves in the microwave to millimeter-wave range are suitable for accessing plasma. In reflectometry, the Ka band (26–40 GHz), Q band (33–50 GHz), and U band (40–60 GHz) cover the ordinary mode (O-mode) cutoff (f_p), and the V band (50–75 GHz), E band (60–90 GHz), and W band (75–110 GHz) cover the extraordinary mode (X-mode) right-hand cutoff (f_r). On the other hand, the probe frequency for scattering measurements must reach deep into the plasma. Therefore, it is extremely important that no electron cyclotron resonance layer or reflection layer exists within the plasma confinement region along the line of sight. For this reason, the W-band (90 GHz) with O-mode polarization is optimal as the probe frequency. This situation varies with magnetic field strength, and particularly in low-magnetic field experiments, higher-frequency D-band (~ 140 GHz) are also used as probe signals.

Doppler reflectometry [4–6], also called Doppler back-scattering [7, 8], is a combination of back-scattering and reflectometry methods. It has a high spatial resolution and allows the observation of turbulence flow velocity and the radial electric field based on the Doppler shift frequency. When a probing microwave beam is injected into a plasma and approaches a cutoff layer with an oblique angle to the

cutoff surface, as illustrated in Fig. 3(a), back-scattering occurs due to density fluctuation. This scattering matches the Bragg condition [7, 8], namely $k = -2k_i$ (where k_i is the local wave vector of the probing beam). A Doppler-shifted frequency ($\omega_D = \mathbf{v} \cdot \mathbf{k} = v_{\perp}k_{\perp} + v_{\parallel}k_{\parallel} + v_r k_r$, where the subscripts \parallel and r indicate the parallel and radial directions, respectively) spectrum is obtained, as shown in Fig. 3(b). It can be typically assumed that $k_{\perp} > k_{\parallel}$ and $v_{\perp} < v_{\parallel}$, and thus the second term ($v_{\parallel}k_{\parallel}$) is negligible in comparison with the first term ($v_{\perp}k_{\perp}$). In addition, if the turbulence is not displaced radially, the third term vanishes and $\omega_D \approx v_{\perp}k_{\perp}$. Then, the perpendicular velocity v_{\perp} of the selected fluctuation can be calculated. The perpendicular velocity is a composition of the plasma background $\mathbf{E} \times \mathbf{B}$ velocity $v_{E \times B}$ and the intrinsic phase velocity of the density fluctuation v_{ph} (i.e., $v_{\perp} = v_{E \times B} + v_{ph}$). If v_{ph} is known or $v_{ph} \ll v_{E \times B}$ (which is usually satisfied at the plasma edge in magnetically confined devices), the radial electric field E_r can be extracted from the measurement of the perpendicular velocity using $v_{\perp} \approx v_{E \times B} = (E_r \times B)/B^2$, where B is the absolute value of the magnetic field. In addition, the intensity of the scattered waves at this time is an indicator of the magnitude of turbulence (density fluctuation).

In this paper, we describe the Doppler reflectometer and scattering system in the LHD. Section "Location of

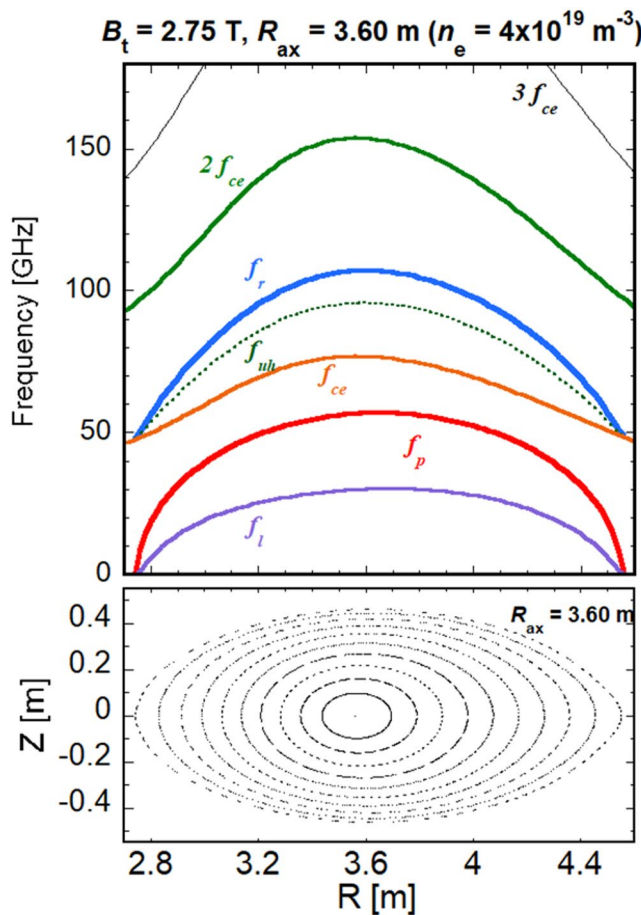


Fig. 2 Radial profiles of characteristic frequencies (top) and magnetic flux surfaces in horizontal plasma cross section (bottom). f_{ce} , $2f_{ce}$, $3f_{ce}$, f_p , f_r , f_l , and f_{uh} are the fundamental, second harmonic, and third harmonic electron cyclotron frequencies, electron plasma frequency, right-hand cutoff frequency, left-hand cutoff frequency, and upper hybrid frequency, respectively. In the measurement, the microwaves access the plasma from the right side of this figure (low-magnetic-field side). For millimeter-wave scattering measurement at 90 GHz with O-mode polarization, the plasma center can be accessed because there is no $2f_{ce}$ absorbing layer

"Doppler reflectometer and scattering system in Large Helical Device" gives the location of each system and its characteristics. Section "Doppler reflectometer" describes the three types of developed Doppler reflectometer system. Section "Millimeter-wave scattering system" describes the millimeter-wave scattering system that utilizes the W and D bands. Finally, Sect. "Conclusions" provides a summary.

Location of Doppler Reflectometer and Scattering System in Large Helical Device

Two toroidally separated ports, namely the 9-O and 3-O ports, are used for microscale turbulence observation, as shown in Fig. 4. These two ports are each equipped with

a Doppler reflectometer with approximately the same field of view. This allows a toroidal correlation analysis of turbulence. The respective fields of view are shown in Fig. 5. In plasma experiments, beam orbits and observation positions are obtained from ray tracing calculations using the LHDGauss code [9, 10] based on electron temperature and density distributions obtained from Thomson scattering measurements at each time slice. Examples of Doppler reflectometer data are shown in Fig. 6. As shown in the 30 GHz example in Fig. 6, setting the same frequency on both ports enables observation at similar minor radius locations.

The millimeter-wave scattering system is also installed in the 3-O port. It has three receivers in a vacuum vessel, allowing simultaneous observations at different angles and different positions relative to the line of sight of the probe. Receiver 1 is a movable antenna, allowing shot-by-shot observations at any position. A detailed description is given in Sect. "Millimeter-wave scattering system".

Doppler Reflectometer

The Doppler reflectometer is used for the study of ion-scale microscale turbulence such as Ion Temperature Gradient/Trapped Electron Mode (ITG/TEM) in the LHD, targeting turbulence with wave numbers $k = 2\text{--}20 \text{ cm}^{-1}$. Several experimental observations of dynamic transport and abrupt phenomena have been reported [11–16].

Frequency-hopping Doppler Reflectometer System

A schematic diagram of the Ka- and V-band Doppler reflectometer system [17] is shown in Fig. 7. A microwave synthesizer (Phase Matrix, QuickSyn FSW-0020) is used as a source because its phase noise is sufficiently low for density fluctuation measurements. The frequency range is 12.5 to 18.0 GHz. Although frequency scanning can be conducted in steps (called a hopping operation), it is usually conducted at a constant frequency during plasma discharge. The output frequency can be easily changed via USB control. The source output is split into the probe signal and the reference signal. The probe signal is multiplied by two and four by an active multiplier to increase the launch frequency for the Ka and V bands, respectively. Each microwave is injected into the plasma from the launch antenna with either O-mode or X-mode polarization. The returning back-scattered wave is received and mixed with the reference wave. To obtain the complex frequency components and the phase fluctuation, single-sideband modulation is used [18]. The single-sideband modulator, which is driven by a 220-MHz (f_m) quartz oscillator, shifts the frequency of the reference signal for heterodyne I-Q detection. In this system, the suppression

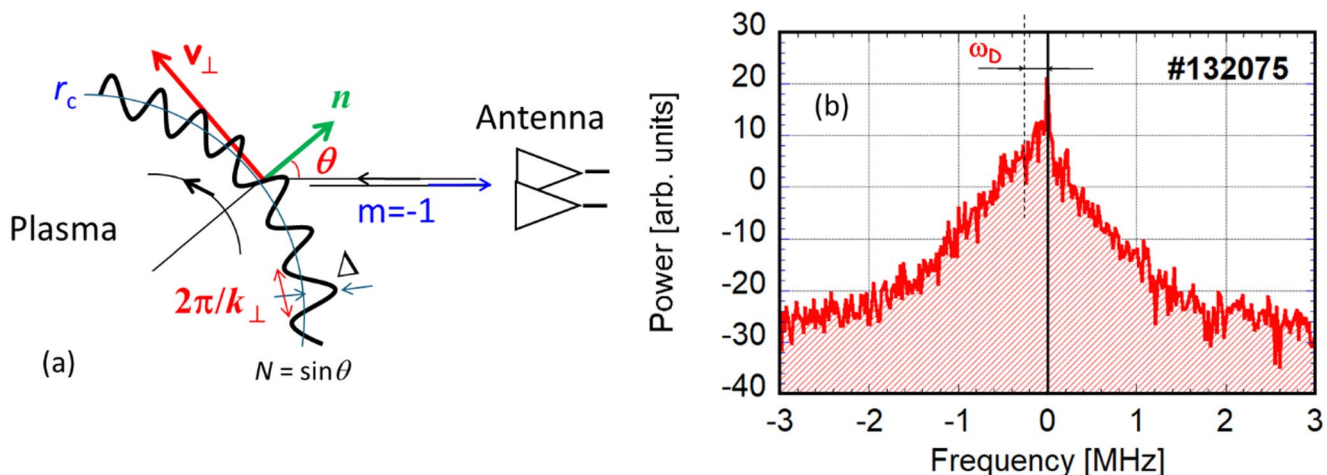
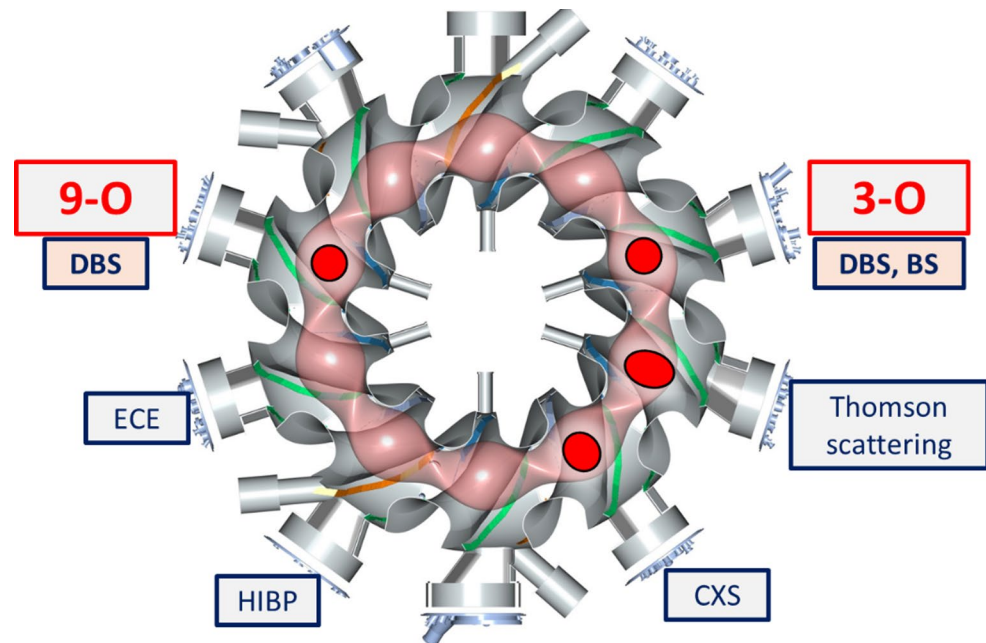


Fig. 3 (a) Schematic diagram of Doppler reflectometry principle. The microwaves are launched at a non-zero tilt angle θ with respect to the normal to the reflecting layer (r_c). The selected perturbation with a finite wave vector component on the reflecting layer k_\perp via microwave

scattering to a diffraction order of -1 is received. (b) Example of Doppler-shifted frequency spectrum obtained by Doppler reflectometer in LHD. ω_D is the Doppler shift frequency estimated by fitting with a Gaussian function

Fig. 4 Doppler reflectometers (DBS) installed at 9-O and 3-O ports and millimeter-wave scattering system (BS) installed at 3-O port. The locations of other major instruments, namely Thomson scattering, charge exchange spectroscopy (CXS), heavy ion beam probe (HIBP), and electron cyclotron emission (ECE), are also shown



levels of the image sidebands are less than -20 dB. The intermediate frequency signal is amplified and filtered by a band-pass filter (BPF) whose pass frequency component is 440 ± 10 MHz or 880 ± 10 MHz. The intermediate frequency signal and the modulation signal are then fed to the I-Q detector. The output signals of the I-Q demodulator, which are denoted as $A\cos\varphi$ and $A\sin\varphi$, are acquired using a real-time data acquisition system consisting of two compact PCI digitizers, whose sampling rates are 10 MHz throughout the plasma discharge.

This reflectometer system, which is located at the 9-O port, went into operation in the 13th cycle of 2009 with shot number 94,600.

Frequency Comb Doppler Reflectometer System

The Ka-band [19] and U-band [20] microwave frequency comb Doppler reflectometer system is shown in Fig. 8. A passive, nonlinear transmission line (Picosecond Pulse Labs, model 7112) modulated by a stable signal generator is used as the frequency comb source. Nonlinear transmission lines, which have excellent low phase noise performance [7, 8], generate an array of equally spaced (presently, $\Delta f = 0.71$ GHz for the Ka band and 1.0 GHz for the U band) frequencies with a slow decay in output microwave power. The output microwave is amplified and subsequently multiplied by each frequency active multiplier in the Ka and U

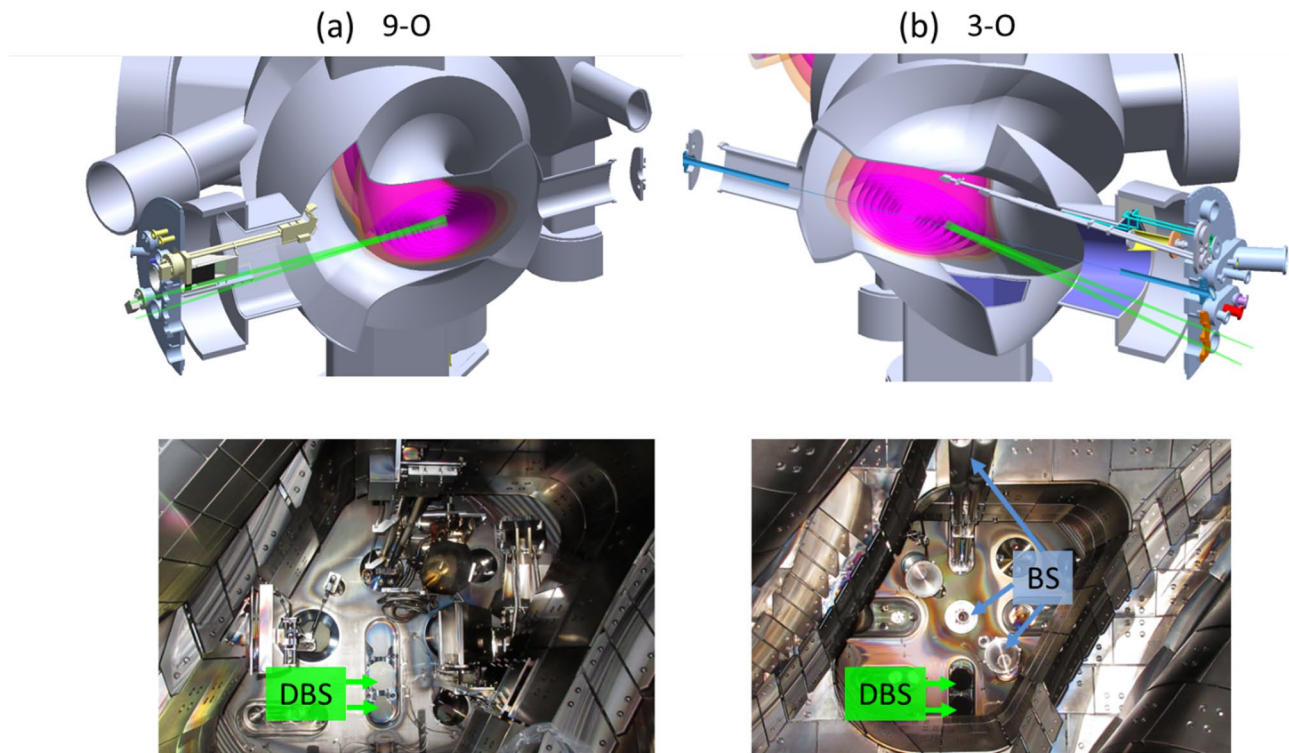


Fig. 5 Cross-sectional view of (a) 9-O port and (b) 3-O port. The Doppler reflectometer antennas are located outside the vacuum vessel. Beam rays (green lines) are shown for reference

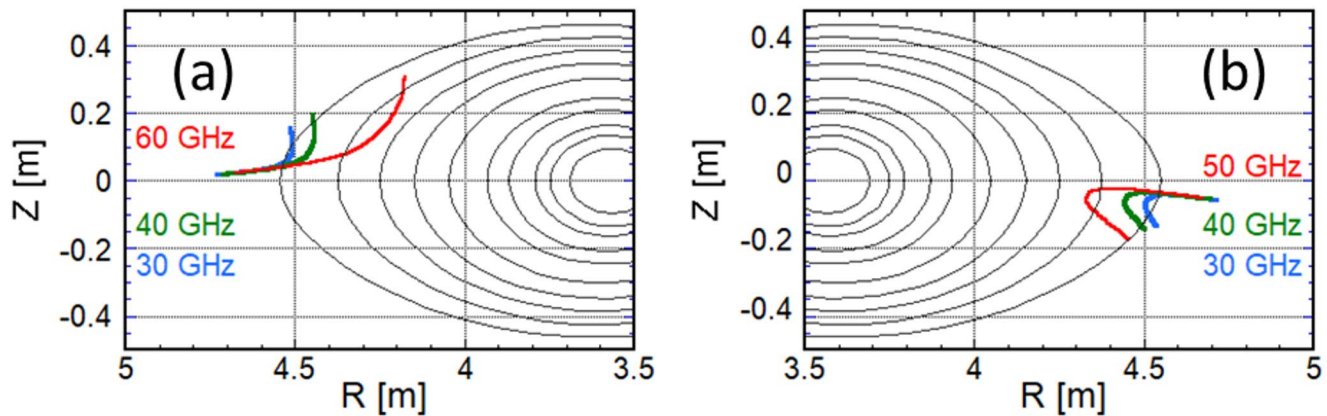


Fig. 6 Example of beam trace calculated using LHDGauss code in horizontal plasma cross section of (a) 9-O port and (b) 3-O port. Note that the launch angle can be changed by adjusting the antenna

bands, respectively. For the Ka band, the number of comb components is around 20 (i.e., 14 GHz/0.7 GHz). Therefore, 20 frequency components can be simultaneously launched into the plasma. A probe beam that combines two band frequency components via a 3 dB directional coupler is launched and received by bistatic conical horn antennas with a lens. These antennas can modify the launch angle to the plasma. The antenna angle is slightly tilted toward the normal of the plasma surface in the horizontal cross section for Doppler reflectometry operation. The Doppler-shifted

back-scattered signal is received and mixed with each local wave, whose frequency is 32.84 GHz for the Ka band and 49.76 GHz for the U band. A portion of the probe wave is divided and fed to a mixer (M1) to form the reference signal (see Fig. 8) for high-sensitivity heterodyne detection.

The down-converted intermediate frequency signals are divided into eight signals and fed to a filter bank system. For the Ka band, the center frequencies of the BPFs are 5.10, 3.70, 2.30, 0.88, 0.53, 1.95, 4.08, and 5.5 GHz with a 200 MHz bandwidth; the corresponding microwave frequencies

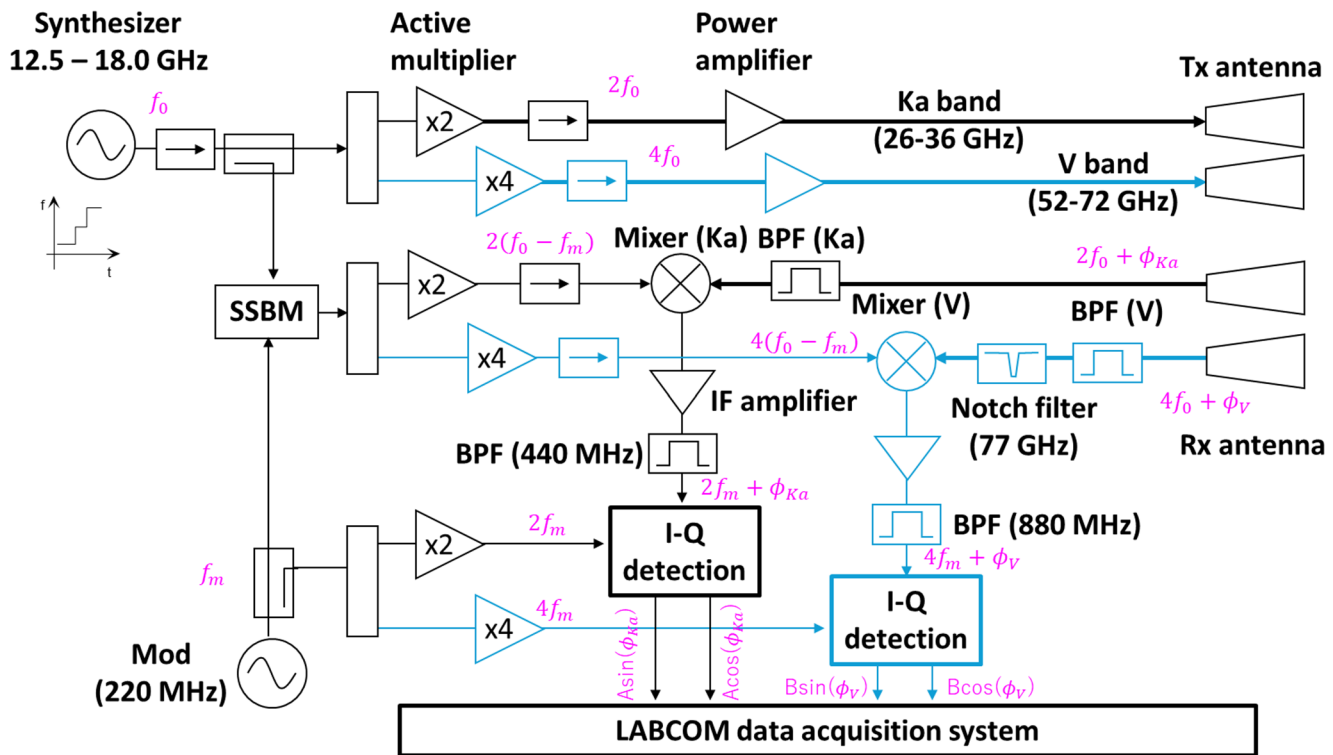


Fig. 7 Schematic diagram of Ka- and V-band frequency-hopping microwave Doppler reflectometer. The V-band component is shown by the blue line. Mod: the source of modulation. SSBM: single-sideband modulator

are 27.69, 29.11, 30.53, 31.95, 33.37, 34.79, 36.92, and 38.34 GHz, respectively. For the U band, the center frequencies of the BPFs are 0.75, 1.25, 2.75, 3.25, 4.75, 5.25, 6.75, and 7.25 GHz; the corresponding microwave frequencies are 43.0, 45.0, 47.0, 49.0, 51.0, 53.0, 55.0, and 57.0 GHz, respectively. Each individual wave passing through a BPF is fed to an I-Q mixer that outputs two signals that are in-phase and quadrature-phase in the I-Q detection section. Finally, the data of the filter bank system are acquired by an analog-to-digital converter with a 1-MHz sampling rate and a 16-bit resolution. In addition, a portion of the probe signal is fed to an electro-optical converter set (E/O and O/E, whose frequency range is 0.1–12 GHz) and transmitted via a 100-m optical fiber directly to a wideband digital oscilloscope (Teledyne LeCroy, WaveMaster 820Zi-B) with four-channel operation, a sampling rate of 80 GS/s, a bandwidth of 20 GHz, and a memory size of 256 Mpts/channel [21].

Figure 9 shows an example of the spatio-temporal structure of turbulence obtained using the multi-frequency channel of the frequency comb Doppler reflectometer. The figure suggests that a fine structure may exist in the microscale

turbulence intensity and Doppler shift frequency. Although the existence of such a structure has been theoretically predicted [22], experimental verification of this structure was made possible by the application of this measurement method.

The Ka-band system became operational in the 16th cycle of 2012 with shot number 112,800 and the U-band system became operational in the 18th cycle of 2014 with shot number 127,500. This system is located at the 3-O port.

Dual-comb Doppler Reflectometer System

A dual-comb system [23, 24] with multi-frequency channels but a reduced intermediate frequency is described below.

When the frequency combs created with a 710-MHz (f_1) clock and a 730-MHz (f_2) clock are input to the mixer as radio-frequency (RF) and local oscillator (LO) signal, respectively, the mixer outputs $|mf_1 - nf_2|$ frequency components (where m and n are integers greater than or equal to 0) that form a frequency chain arranged at 20-MHz

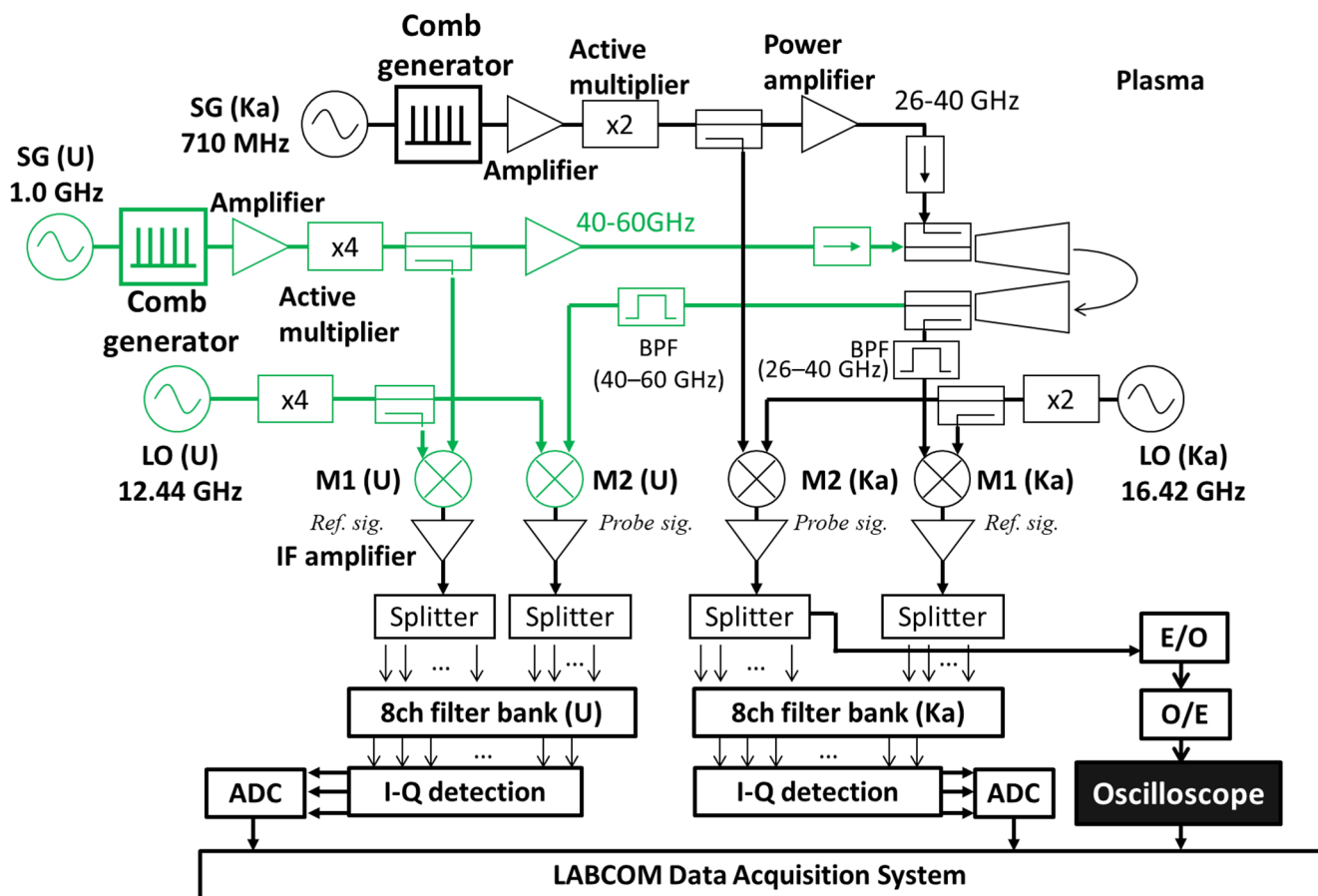


Fig. 8 Schematic diagram of Ka- and U-band frequency comb Doppler reflectometer. The U-band component is shown by the green line. SG: signal generator. LO: local oscillator. M1 and M2: mixer

intervals. This is the concept of the dual-comb method. The intermediate frequency bandwidth is expected to be significantly reduced compared with that of the frequency comb system described above.

The Ka-band dual-comb Doppler reflectometer system is shown in Fig. 10. The comb sources are operated at 710 and 730 MHz, respectively. A frequency of 710 MHz was chosen because the RF frequencies of the probing match the frequencies of the existing Doppler reflectometer system described above, allowing correlative measurements at two separate toroidal locations. The output frequency components are doubled to obtain the probing Ka-band range. One of the frequency comb components is input into the LO port of Mixer 1 through a BPF with a center frequency of 26.27 GHz with a ± 150 -MHz bandwidth. Then, the output of Mixer 1 is combined with the frequency comb components from Comb Generator 2 at Mixer 3 to generate the

probe signal. For precise heterodyne detection, parts of the signals from Comb Generator 1 and Comb Generator 2 components are mixed in Mixer 2 to generate a frequency chain for use as the reference signal for I-Q detection. I-Q detection is performed by fabricating the receiving circuit on a single substrate board together with a filter bank for each of the four frequencies as shown in Fig. 11. The BPF center frequencies of the filter bank in this system are 0.04, 0.08, 0.12, 0.16, 0.20, 0.24, 0.30, and 0.34 GHz, an order of magnitude lower than those of the system described above. This system collects a portion of the signal directly on a digital oscilloscope (Teledyne LeCroy, WavePro 254HD), but its frequency bandwidth is 2.5 GHz, which is narrower than that of the previous section.

This dual-comb Doppler reflectometer system went into operation in the 20th cycle of 2018 with shot number

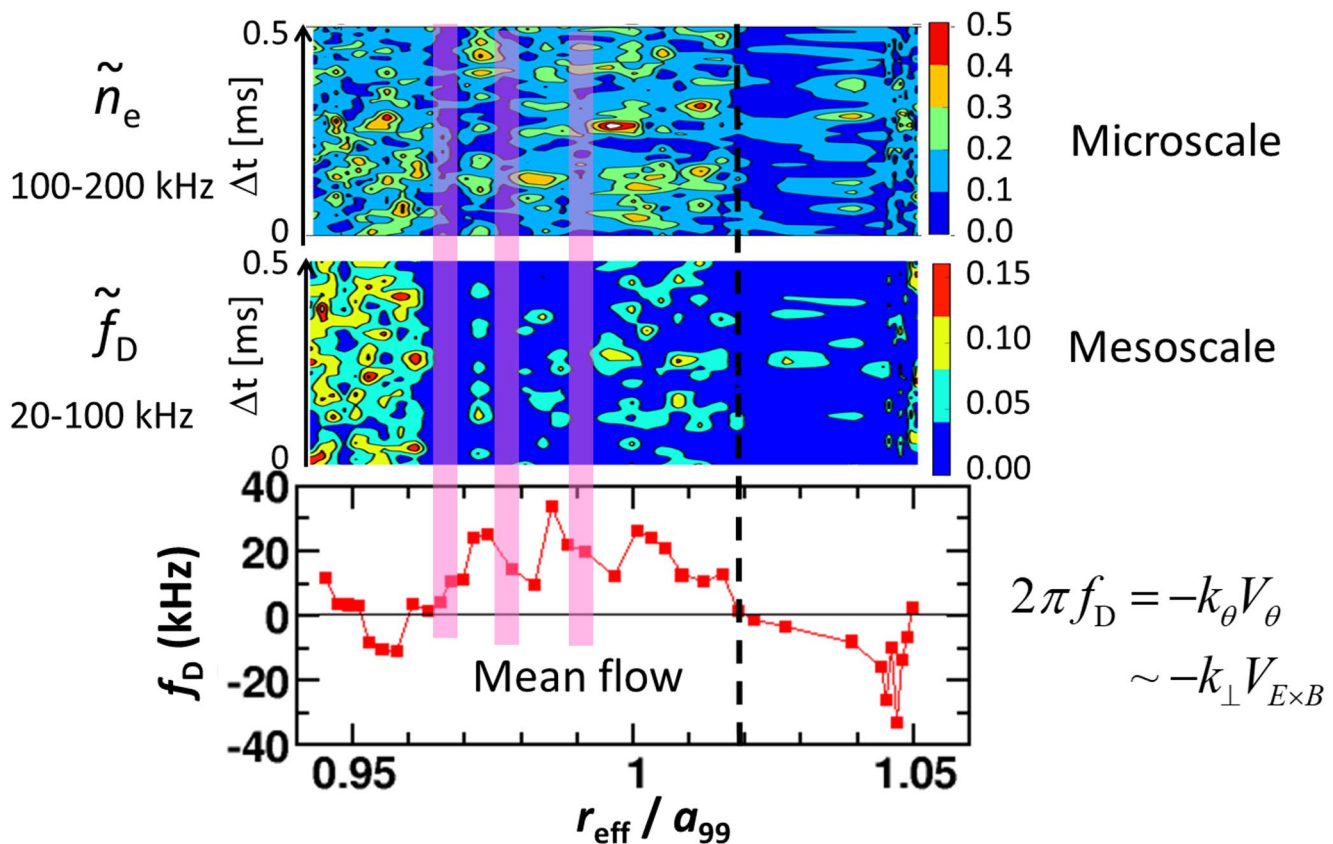


Fig. 9 Spatio-temporal structure of microscale turbulence intensity (top) and Doppler shift frequency (middle). Radial profile of Doppler shift frequency (bottom). The detailed spatial structure of such turbulence could be observed for the first time

148,000. This system is operated with a 3-O port antenna shared with the hopping reflectometer system.

Millimeter-wave Scattering System

The W- and D-band millimeter-wave scattering system was installed to observe finer microscale turbulence at wave numbers $k=25\text{--}40\text{ cm}^{-1}$. As shown in Fig. 1, applying back-scattering at angles even larger than 90° in these frequency regions allows for higher-wavenumber turbulence observations.

Figure 12 shows the arrangement of antennas for the millimeter-wave scattering system installed in the 3-O port. The antenna installed in the horizontal plane port of the horizontal cross section is used for the millimeter-wave launcher. This antenna is also used for the millimeter-wave interferometer [25]. A labyrinth waveguide is installed at the opposite side of the vacuum vessel. Three receiving antennas

(Receivers 1–3) are installed inside the vacuum vessel. Receiver 1 is a movable antenna that can realize a scattering angle of $159^\circ \pm 6^\circ$ and Receivers 2 and 3 are fixed antennas at around 100° and 90° , respectively. All receiving antennas have a focusing function, with the focusing system based on a metal lens for Receiver 1 [26] and a rotating parabolic mirror for Receivers 2 and 3. The positional relationship in the vacuum vessel is shown in Fig. 13, where Receivers 2 and 3 are set to focus at $R = 4.0$ and 4.4 m, respectively, in the horizontal plane. Thus, Receiver 1 observes turbulence with a component in an almost major radius direction (R-direction) and Receivers 2 and 3 observe turbulence roughly half in the Z-direction and half in the R-direction, allowing turbulence anisotropy to be examined. Furthermore, probe beams with different frequencies (90 GHz and around 140 GHz) can be used to observe turbulence with different vectors but the same wavenumber. To launch probe beams with different frequencies from a single antenna into the plasma, a coupling system with a dichroic filter was constructed, as

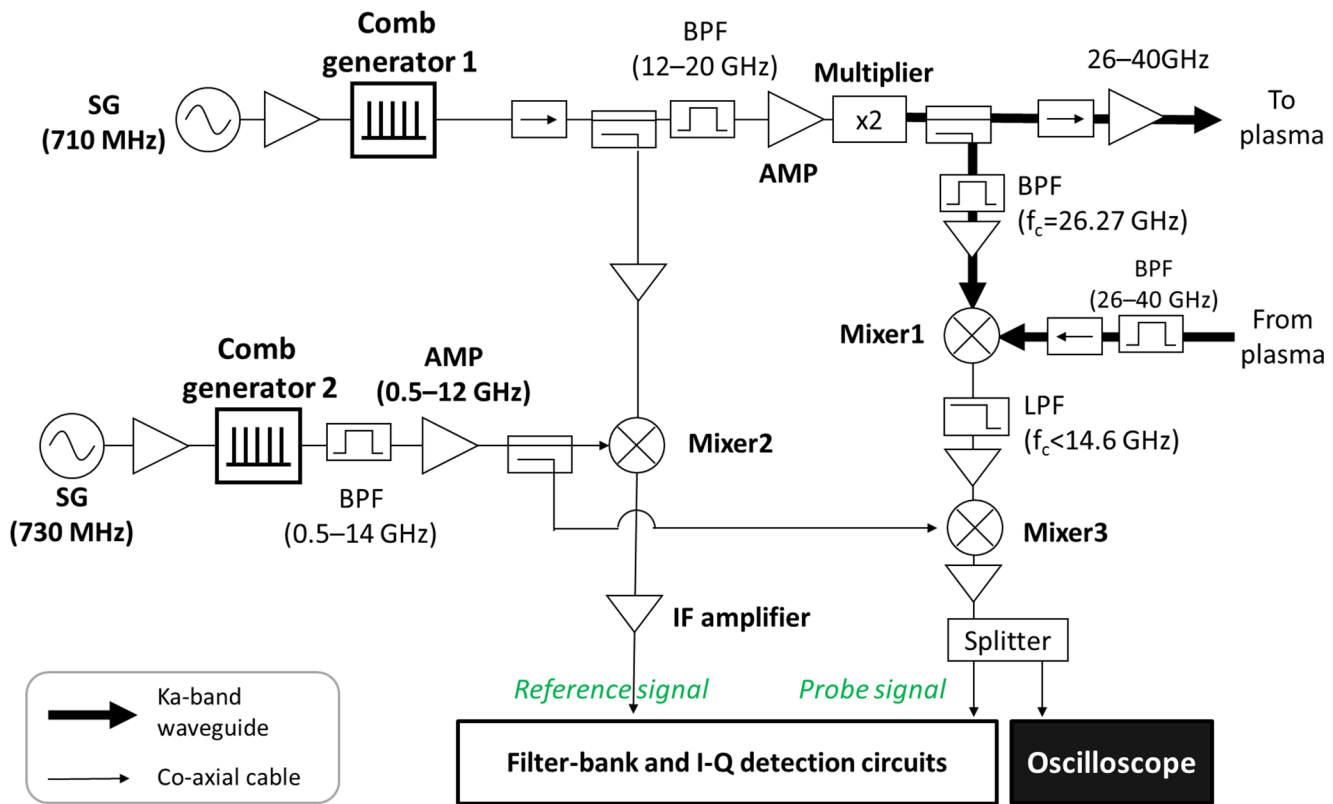


Fig. 10 Schematic diagram of dual-frequency comb Doppler reflectometer. SG: signal generator, LPF: low-pass filter

shown in Fig. 14. The two types of dichroic filter (see Fig. 14(b)), which have holes with diameters of 1.6 and 1.0 mm, respectively, function as high-pass filters. Their respective frequency responses when placed at a 45° angle are shown in Figs. 14(c) and (d), respectively. The obtained cutoff frequency is as designed. The millimeter waves in the three bands are efficiently coupled.

The millimeter-wave circuit for the two-frequency scattering system is shown in Fig. 15. Since precise density fluctuation measurements require a low-noise source for the probing beam, a dielectric resonator oscillator with a synchronized quartz oscillator is used as the source for the W-band system. For the D-band system, a synthesizer (BNC, 825-M-20-2) with a variable frequency is as the source. The desired W- and D-band probe frequencies are obtained using active multipliers (6 \times and 12 \times multipliers, respectively). Local oscillators are also provided. Heterodyne detection is performed for I-Q detection. Each output of I-Q detection is fed to analog-to-digital convertors (National Instruments, PXI-6115) that have a sampling rate of 2.5 MHz. The LABCOM data acquisition system [27]

collects the acquired signal in real-time. The acquisition settings are controlled via the associated web site.

The main noise in the plasma experiments conducted using this system is considered to be electron cyclotron emission radiation. To estimate its noise level, the power of the probe wave is modulated by a single-pole single-throw switch. Figure 16 shows an example of an observed frequency spectrum. Electron cyclotron emission radiation noise, which has broad frequency components, is detected but the scattered signal is found to be sufficiently large for fluctuation measurements.

With this scattering system, various studies have characterized microscopic turbulence. Recently, the dependence of turbulence intensity on the electron temperature gradient has been determined [28], as shown in Fig. 17. New findings include the fact that the turbulence intensity increases rapidly above a certain temperature gradient and that turbulence at this high wavenumber exists even for very small temperature gradients. This system has also been used in studies on electron-scale turbulence response [29–31].

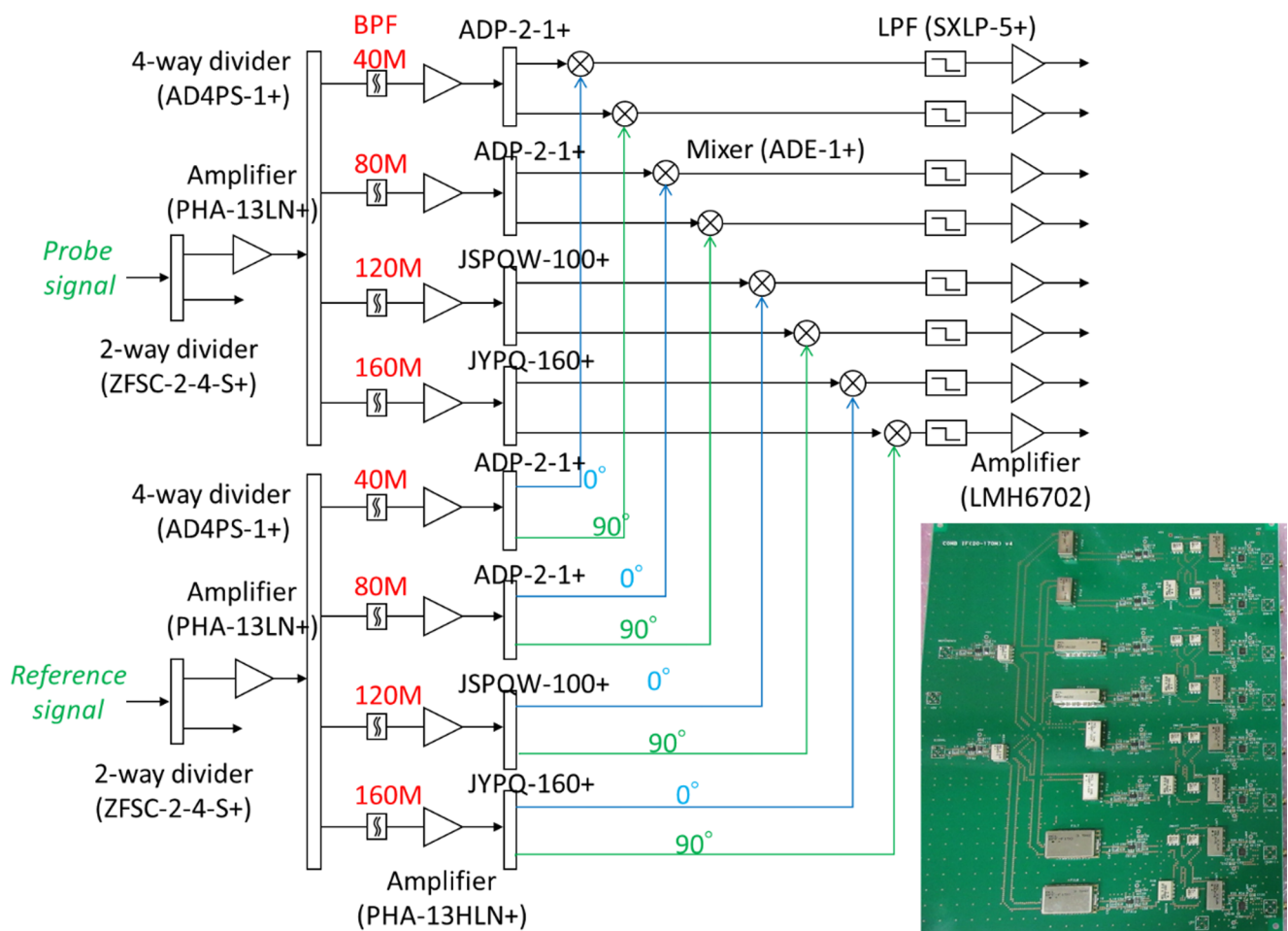


Fig. 11 Schematic circuit diagram and photograph (inset) of filter bank for frequencies of 40, 80, 120, and 160 MHz

In addition, taking advantage of the ability to observe at the same plasma location as the Doppler reflectometer described in Sect. "Doppler reflectometer", the characteristics and interactions of turbulence in various wavenumber regions are currently being studied. Figure 18 shows the frequency spectrum of turbulence at various wavenumbers. It can be seen that even at the same location, the observed

wavenumber regions are different, resulting in completely different frequency spectra.

The W-band system became operational in the 20th cycle of 2018 with shot number 146,500 and the D-band system became operational in the 25th cycle of 2024 with shot number 188,700.

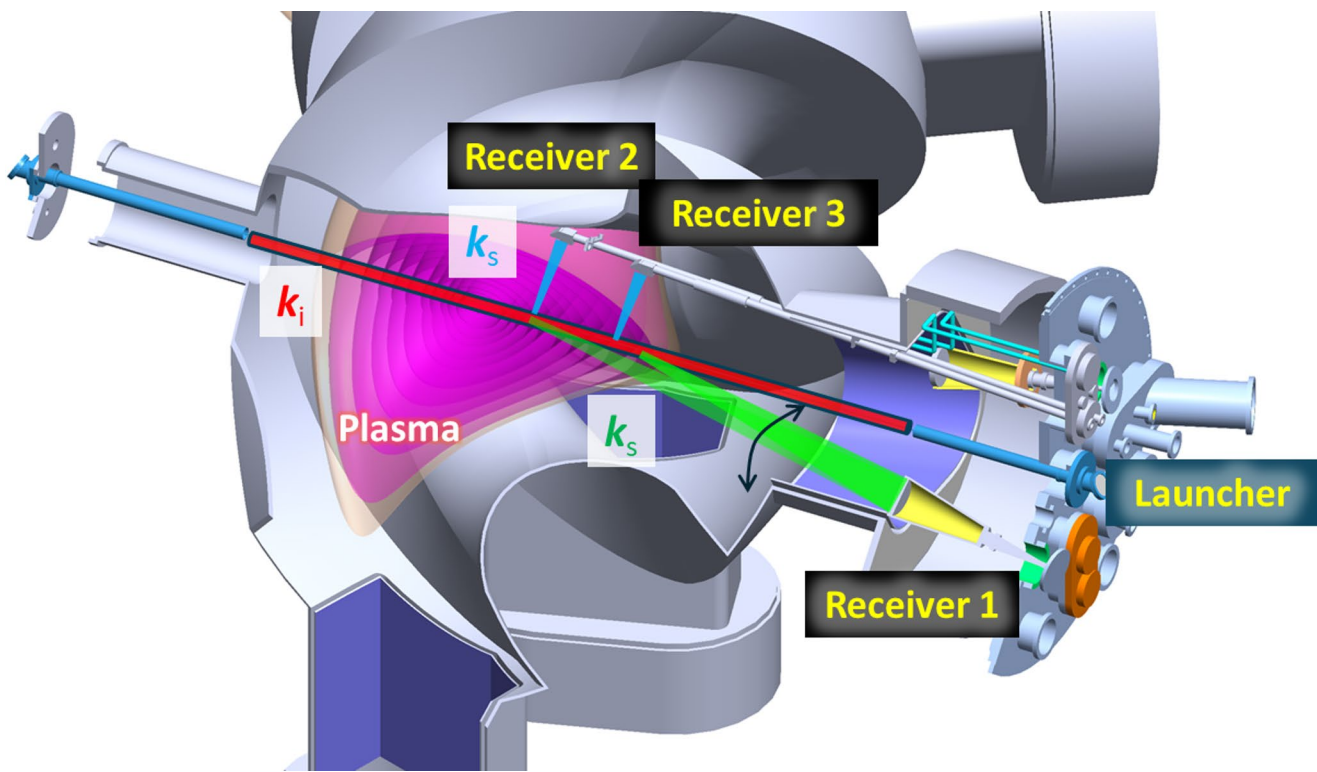


Fig. 12 In-vessel antennas for millimeter-wave scattering system, one for launcher and three for receiver. Here, the plasma shape is illustrated by the magnetic surface layers (magenta)

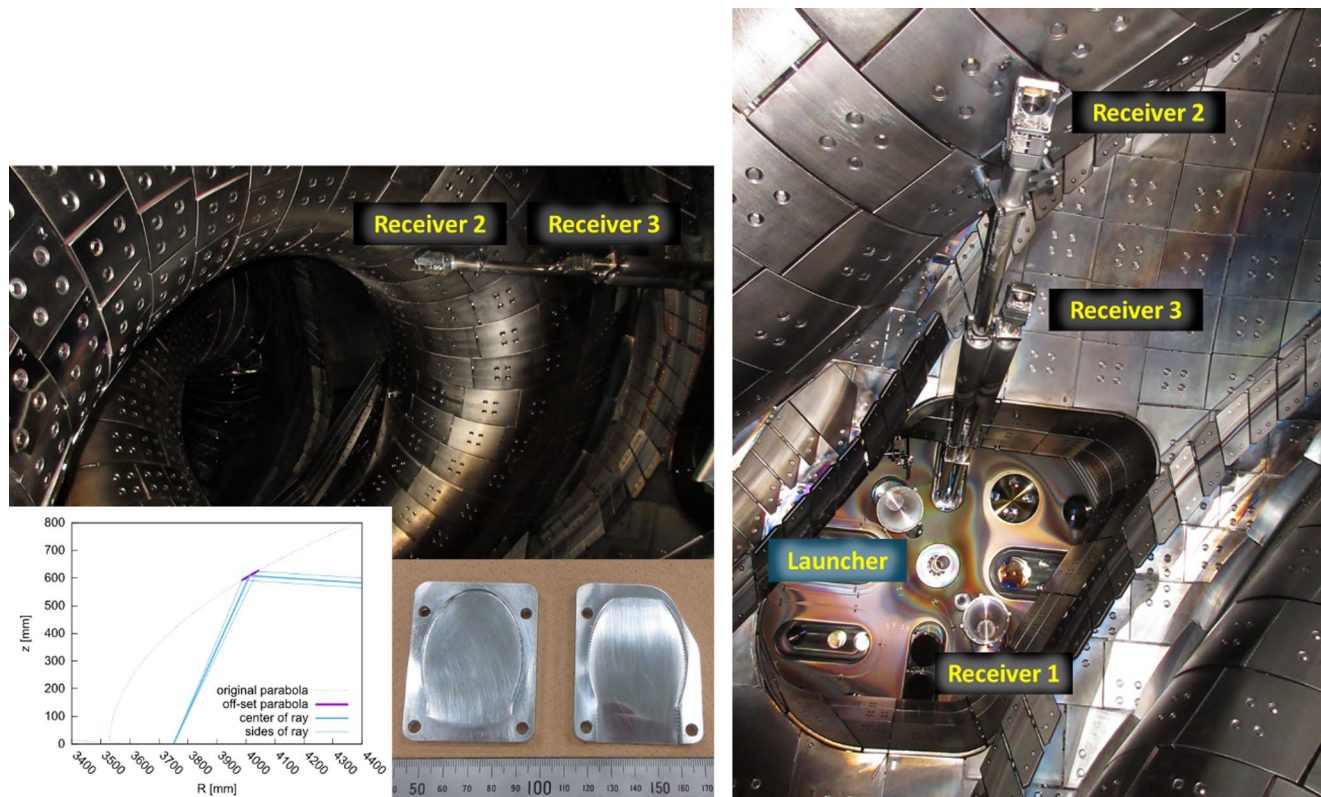


Fig. 13 Photograph of in-vessel antennas installed at 3-O port. The focusing rotating parabolic mirrors used for Receivers 2 and 3 are shown in the inset

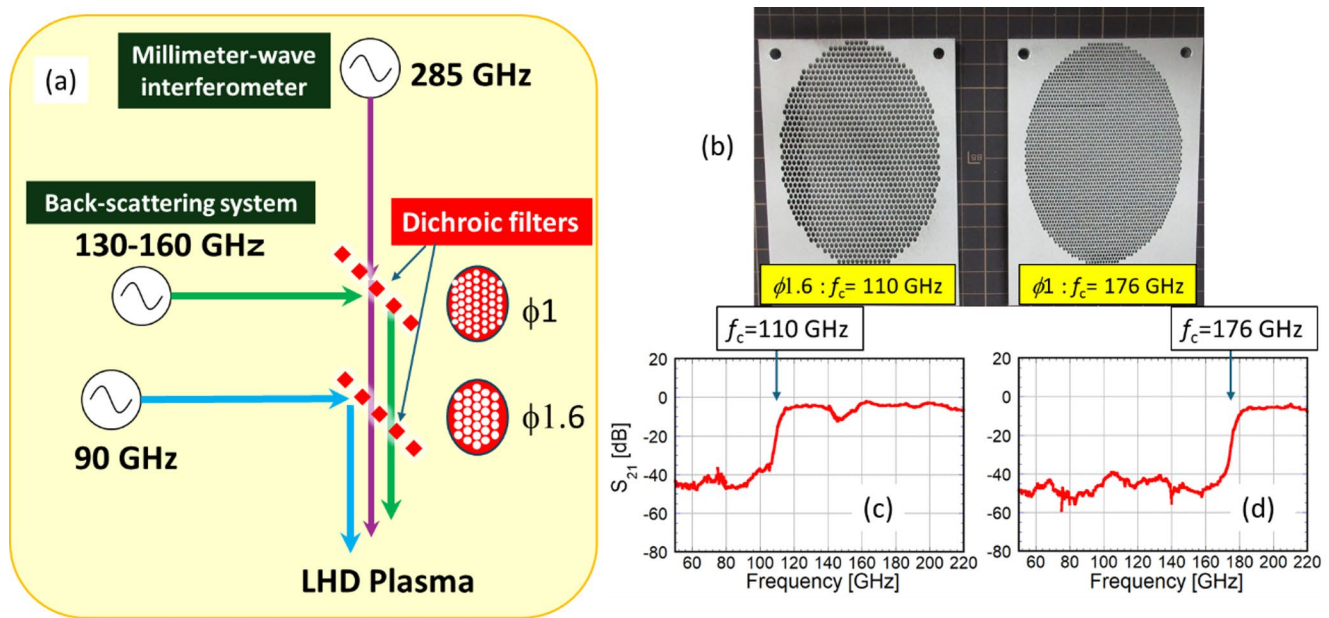


Fig. 14 (a) Schematic diagram of the coupling of three frequency signals. (b) Photograph of dichroic filters. Transmission frequency characteristics of (c) $\phi 1.6$ -mm filter and (d) $\phi 1.0$ -mm filter. The 140 GHz signal is reflected by the $\phi 1.0$ -mm filter and transmitted by the $\phi 1.6$ -mm filter

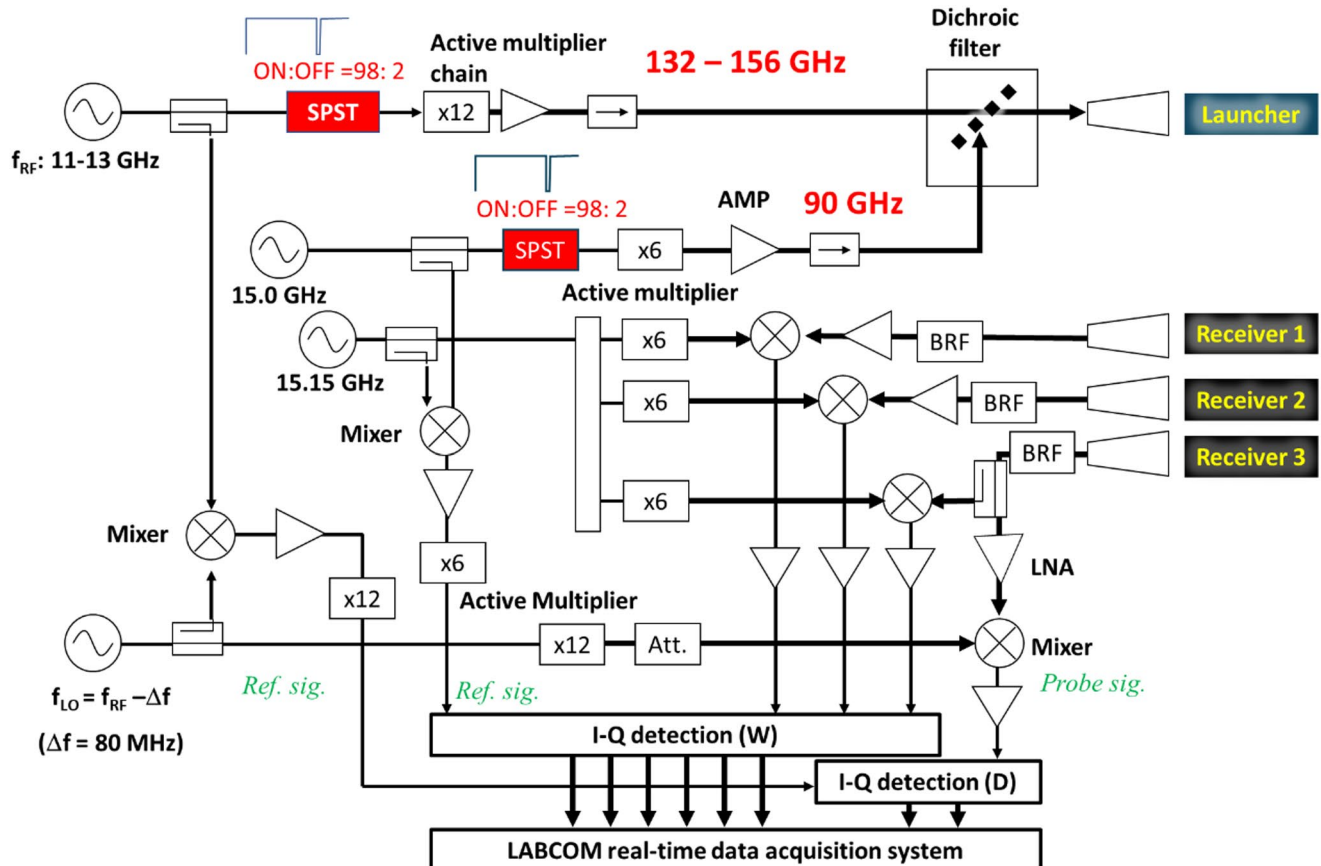


Fig. 15 Schematic diagram of W-band (90 GHz) and D-band millimeter-wave scattering system. SPST: single-pole single-throw. BRF: band rejection filter with center frequency of 154 GHz. LNA: low noise amplifier

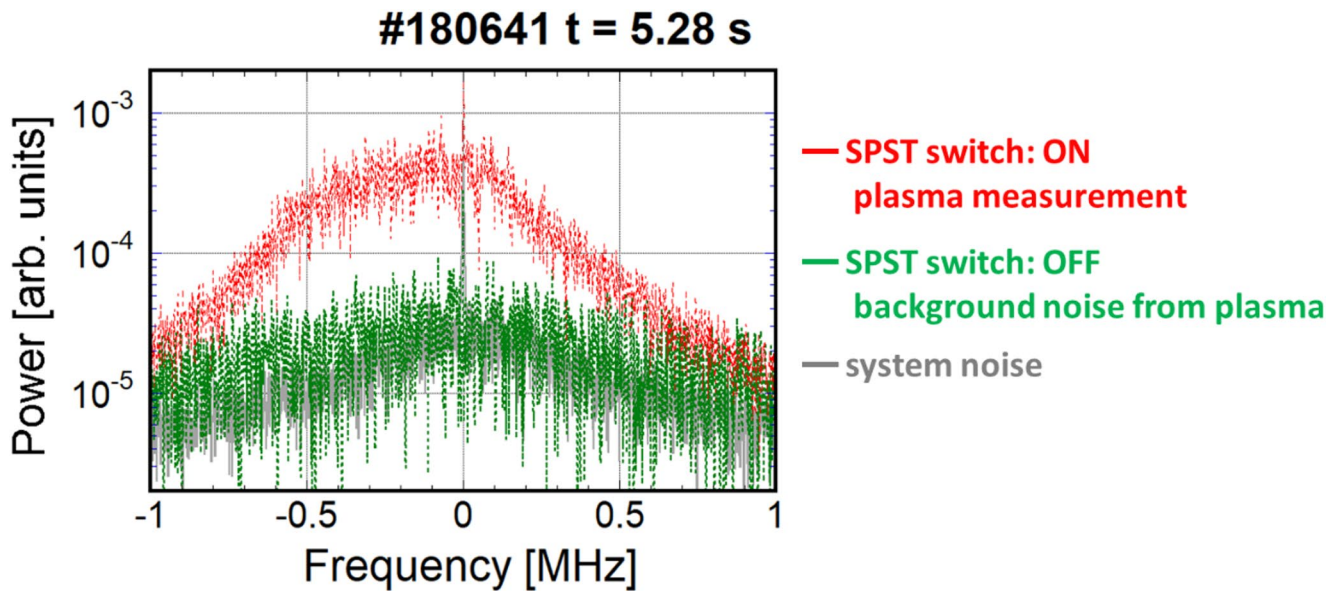


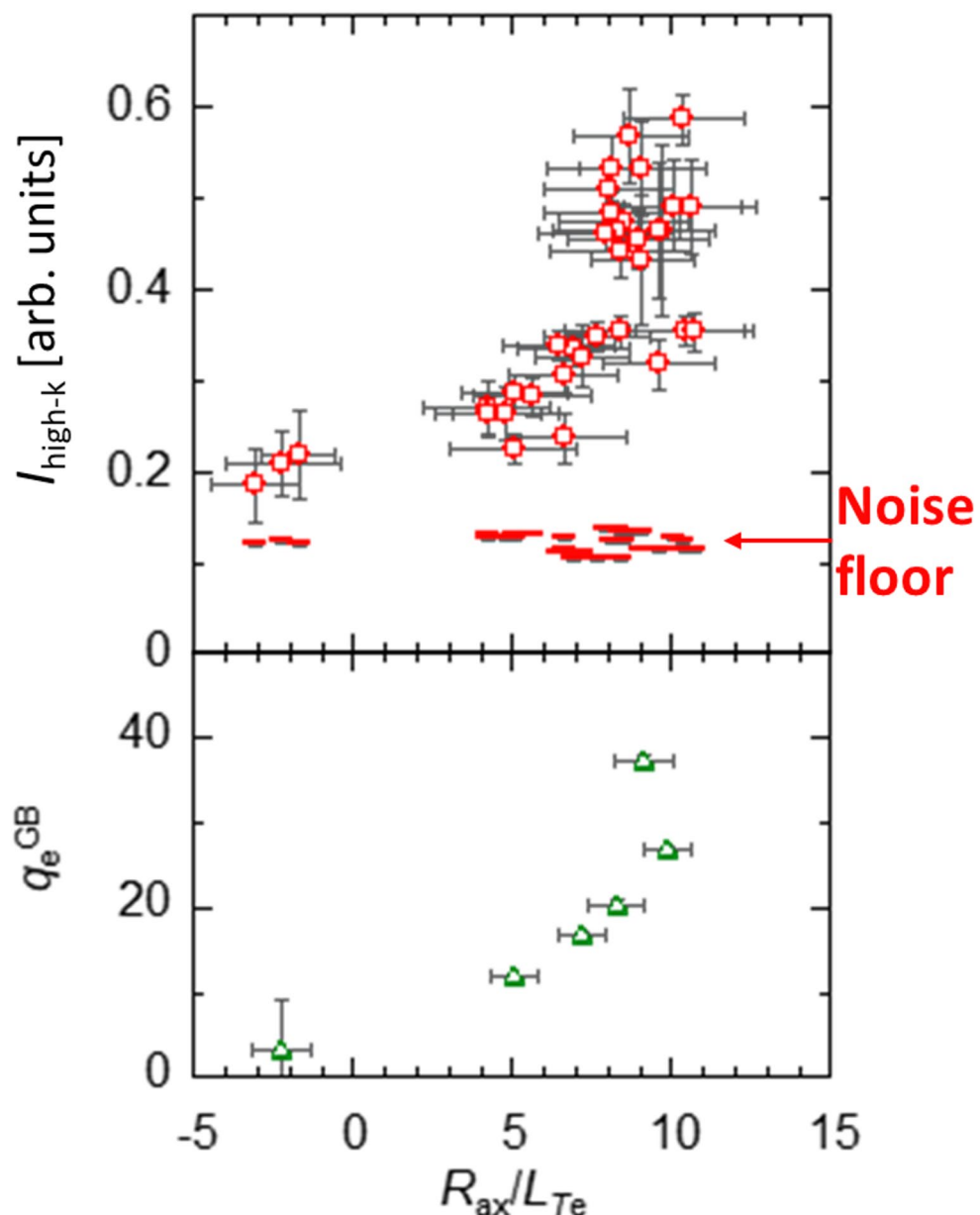
Fig. 16 Example of observed frequency spectrum (red). The green line shows the signal when the single-pole single-throw switch is off and the gray line shows the system noise when there is no plasma

Conclusions

A microwave Doppler reflectometer and a millimeter-wave scattering system were installed at the LHD for observing

microscale turbulence with high temporal and spatial resolutions. For the Doppler reflectometer, a system with three types of circuit was constructed to allow simultaneous

Fig. 17 Dependence of (top) higher wavenumber microscale turbulence intensity and (bottom) gyro-Bohm normalized electron-heat flux on R_{ax}/L_{T_e}



multi-point spatial measurements. A millimeter-wave scattering system was developed to observe microscale turbulence at relatively high wavenumbers. This system has been used to study response differences between turbulence at

different scales and turbulence anisotropy. The combination of these two diagnostics systems is expected to enable the study of multi-scale turbulent interactions.

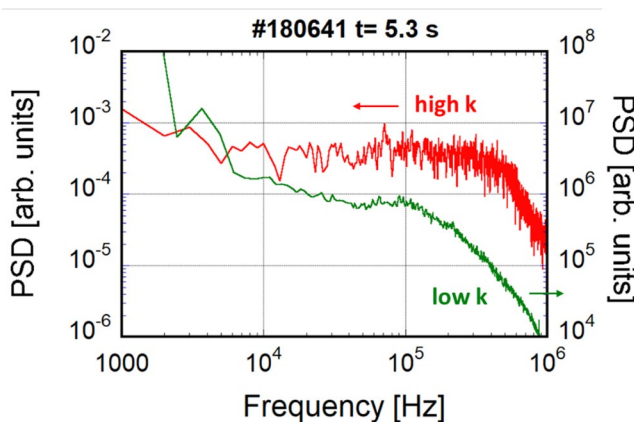


Fig. 18 Examples of frequency spectra of high-wavenumber (red) and low-wavenumber (green) microscale turbulences at the same location. PSD: power spectral density

Supplementary Information The online version contains supplementary material available at <https://doi.org/10.1007/s10894-025-00523-1>.

Acknowledgements The authors thank the LHD experiment group for their support of this work. This study was supported in part by the Japan Society for the Promotion of Science KAKENHI (grant nos. 23K25858, 23H01161, 21H04973, 19H01880, 17K18773, 17H01368, 15H02335, 15H02336, 26630474, 25289342, 23244113, 23360414, 22360394, 22017007, and 21224014), by a budgetary Grant-in-Aid from the National Institute for Fusion Science (NIFS) LHD project under the auspices of the NIFS Collaboration Research Program, and by the Collaborative Research Programs of the Research Institute for Applied Mechanics, Kyushu University. Additional support was provided by the Japan/U.S. Cooperation in Fusion Research and Development.

The data supporting the findings of this study are available in the LHD experiment data repository at <https://doi.org/10.57451/lhd.analyzed-data>.

Author Contributions T.T. and D.N. wrote the main manuscript text, T. N. prepared figure 17, and S.I. prepared figure 9. All authors reviewed the manuscript.

Data Availability The data supporting the findings of this study are available in the LHD experiment data repository at <https://doi.org/10.57451/lhd.analyzed-data>.

Declarations

Competing Interests The authors declare no competing interests.

Open Access This article is licensed under a Creative Commons Attribution 4.0 International License, which permits use, sharing, adaptation, distribution and reproduction in any medium or format, as long as you give appropriate credit to the original author(s) and the source, provide a link to the Creative Commons licence, and indicate if changes were made. The images or other third party material in this article are included in the article's Creative Commons licence, unless indicated otherwise in a credit line to the material. If material is not included in the article's Creative Commons licence and your intended use is not permitted by statutory regulation or exceeds the permitted use, you will need to obtain permission directly from the copyright

holder. To view a copy of this licence, visit <http://creativecommons.org/licenses/by/4.0/>.

References

1. D.H. Froula, S.H. Glenzer, N.C. Jr. Luhmann, J. Sheffield, *Plasma Scattering of Electromagnetic Radiation* (Academic. 2011)
2. T. Tokuzawa, K. Tanaka, T. Tsujimura, S. Kubo, M. Emoto, S. Inagaki, K. Ida, M. Yoshinuma, K. Watanabe, H. Tsuchiya, A. Ejiri, T. Saito, K. Yamamoto, L.H.D.E. Group, W-band millimeter-wave back-scattering system for high wavenumber turbulence measurements in LHD. *Rev. Sci. Instrum.* **92**, 043536 (2021). <https://doi.org/10.1063/5.0043474>
3. W. Lee, H.K. Park et al., Design of a collective scattering system for small scale turbulence study in Korea superconducting Tokamak advanced research. *Rev. Sci. Instrum.* **87**, 043501 (2016)
4. M. Hirsch, E. Holzhauer, J. Baldzuhn, B. Kurzan, B. Scott, Doppler reflectometry for the investigation of propagating density perturbations. *Plasma Phys. Control. Fusion.* **43**, 1641 (2001). <https://doi.org/10.1088/0741-3335/43/12/302>
5. V.V. Bulanin, S.V. Lebedev, L.S. Levin, V.S. Roytershteyn, Study of plasma fluctuations in the Tuman-3m Tokamak using microwave reflectometry with an obliquely incident probing beam. *Plasma Phys. Rep.* **26**, 813–819 (2000). <https://doi.org/10.1134/1.1316822>
6. G.D. Conway, S. Schirmer, S. Klenge, W. Sutrop, E. Holzhauer, A.S.D.E.X.U. Team, Plasma rotation profile measurements using doppler reflectometry. *Plasma Phys. Control. Fusion.* **46**, 951 (2004). <https://doi.org/10.1088/0741-3335/46/6/003>
7. J.C. Hillesheim, W.A. Peebles, T.L. Rhodes, L. Schmitz, T.A. Carter, P.A. Gourdain, G. Wang, A multichannel, frequency-modulated, tunable doppler backscattering and reflectometry system. *Rev. Sci. Instrum.* **80**, 083507 (2009). <https://doi.org/10.1063/1.3205449>
8. W.A. Peebles, T.L. Rhodes, J.C. Hillesheim, L. Zeng, C. Wannberg, A novel, multichannel, comb-frequency doppler backscatter system. *Rev. Sci. Instrum.* **81**, 10D902 (2010). <https://doi.org/10.1063/1.3464266>
9. S. Kubo et al., ECH power deposition study in the collisionless plasma of LHD, in *Proceedings of 11th Int. Congress on Plasma Physics* (July 2002, Sydney, Australia) p.133 (2002)
10. T.I. Tsujimura et al., Development and application of a ray-tracing code integrating with 3D equilibrium mapping in LHD ECH experiments. *Nucl. Fusion* **55**, 123019 (2015)
11. S. Inagaki et al., How is turbulence intensity determined by macroscopic variables in a toroidal plasma? *Nucl. Fusion* **53**, 113006 (2013). <https://doi.org/10.1088/0029-5515/53/11/113006>
12. H. Takahashi et al., Extension of operational regime in high-temperature plasmas and effect of ECRH on ion thermal transport in the LHD. *Nucl. Fusion* **57**, 086029 (2017). <https://doi.org/10.1088/1741-4326/aa754b>
13. A.J. Creely, K. Ida, M. Yoshinuma, T. Tokuzawa, T. Tsujimura, T. Akiyama, R. Sakamoto, M. Emoto, K. Tanaka, C.A. Michael, Novel analysis technique for measuring edge density fluctuation profiles with reflectometry in the large helical device. *Rev. Sci. Instrum.* **88**, 073509 (2017). <https://doi.org/10.1063/1.4993437>
14. C. Moon, T. Kobayashi, K. Ida, T. Tokuzawa, C. Hidalgo, M. Yoshinuma, K. Ogawa, K. Itoh, A. Fujisawa, LHD Experiment Group, Spatial structure of low-frequency fluctuations throughout the transition of poloidal flow velocity in edge plasmas of LHD. *Phys. Plasmas* **26**, 092302 (2019). <https://doi.org/10.1063/1.5098954>

15. T. Tokuzawa et al., Distorted magnetic island formation during slowing down to mode locking in helical plasmas. *Nucl. Fusion*. **57**, 076003 (2017). <https://doi.org/10.1088/1741-4326/aa6d26>
16. K. Ida, T. Kobayashi, T. Tokuzawa, T. Akiyama, H. Tanaka, M. Yoshinuma, K. Itoh, L.H.D.E. Group, Exhaust of turbulence cloud at the tongue shaped deformation event. *Nucl. Fusion*. **58**, 112008 (2018). <https://doi.org/10.1088/1741-4326/aab971>
17. T. Tokuzawa, A. Ejiri, K. Kawahata, K. Tanaka, I. Yamada, M. Yoshinuma, K. Ida, C. Suzuki, Microwave doppler reflectometer system in LHD. *Rev. Sci. Instrum.* **83**, 10E322 (2012). <https://doi.org/10.1063/1.4733736>
18. T. Tokuzawa, A. Ejiri, K. Kawahata, K. Tanaka, Y. Ito, V-band frequency hopping microwave reflectometer in LHD. *Rev. Sci. Instrum.* **79** (2008). <https://doi.org/10.1063/1.2969036>
19. T. Tokuzawa, S. Inagaki, A. Ejiri, R. Soga, I. Yamada, S. Kubo, M. Yoshinuma, K. Ida, C. Suzuki, K. Tanaka et al., Ka-band microwave frequency comb doppler reflectometer system for the large helical device. *Plasma Fusion Res.* **9**, 1402149 (2014). <https://doi.org/10.1585/pfr.9.1402149>
20. R. Soga, T. Tokuzawa, K.Y. Watanabe, K. Tanaka, I. Yamada, S. Inagaki, N. Kasuya, Developments of frequency comb microwave reflectometer for the interchange mode observations in LHD plasma. *J. Instrum.* **11**, C02009 (2016). <https://doi.org/10.1088/1748-0221/11/02/C02009>
21. T. Tokuzawa, H. Tsuchiya, T. Tsujimura, M. Emoto, H. Nakaniishi, S. Inagaki, K. Ida, H. Yamada, A. Ejiri, K.Y. Watanabe et al., Microwave frequency comb doppler reflectometer applying fast digital data acquisition system in LHD. *Rev. Sci. Instrum.* **89**, 10H118 (2018). <https://doi.org/10.1063/1.5035118>
22. G. Dif-Pradalier, G. Hornung, P. Ghendrih, Y. Sarazin, F. Clairet, L. Vermare, P.H. Diamond, J. Abiteboul, T. Cartier-Michaud, C. Ehrlacher, D. Estéve, X. Garbet, V. Grandgirard, Ö.D. Gürcan, P. Hennequin, Y. Kosuga, G. Latu, P. Maget, P. Morel, C. Norscini, R. Sabot, A. Storelli, Finding the elusive \times staircase in magnetized plasmas. *Phys. Rev. Lett.* **114**, 085004 (2015). <https://doi.org/10.1103/PhysRevLett.114.085004>
23. T. Tokuzawa, S. Inagaki, M. Inomoto, A. Ejiri, T. Nasu, T.I. Tsujimura, K. Ida, Application of dual frequency comb method as an approach to improve the performance of multi-frequency simultaneous radiation doppler radar for high temperature plasma diagnostics. *Appl. Sci.* **12**, 4744 (2022). <https://doi.org/10.3390/app12094744>
24. T. Nasu, T. Tokuzawa, T.I. Tsujimura, K. Ida, M. Yoshinuma, T. Kobayashi, K. Tanaka, M. Emoto, S. Inagaki, A. Ejiri, J. Kohagura, Receiver circuit improvement of dual frequency-comb ka-band doppler backscattering system in the large helical device (LHD). *Rev. Sci. Instrum.* **93**, 113518 (2022). <https://doi.org/10.1063/5.0101588>
25. T. Akiyama, K. Kawahata, K. Tanaka, T. Tokuzawa, Y. Ito, S. Okajima, K. Nakayama, C.A. Michael, L.N. Vyacheslavov, A. Sanin, Tsuji-Iio, interferometer systems on LHD. *Fusion Sci. Technol.* **58**(1), 352–363 (2017). <https://doi.org/10.13182/FST10-8>
26. T. Tokuzawa, K. Tanaka, T. Tsujimura, S. Kubo, M. Emoto, S. Inagaki, K. Ida, M. Yoshinuma, K.Y. Watanabe, H. Tsuchiya, A. Ejiri, T. Saito, K. Yamamoto, L.H.D.E. Group, W-band millimeter-wave back-scattering system for high wavenumber turbulence measurements in LHD. *Rev. Sci. Instrum.* **92**, 043536 (2021). <https://doi.org/10.1063/5.0043474>
27. H. Nakanishi, M. Ohsuna et al., Real-time data streaming and storing structure for the lhd's fusion plasma experiments. *IEEE Trans. Nucl. Sci.* **63**, 222 (2016)
28. T. Nasu, T. Tokuzawa, M. Nakata, K. Ida, S. Inagaki, M. Nishiura, Y. Yoshimura, R. Yanai, K. Tanaka, M. Yoshinuma, T. Kobayashi, A. Ejiri, K.Y. Watanabe, I. Yamada, Electron-scale turbulence characteristics with varying electron temperature gradient in LHD. *Nucl. Fusion*. **64**, 096008 (2024). <https://doi.org/10.1088/741-4326/ad5d7c>
29. K. Tanaka et al., Isotope effects on transport in LHD. *Plasma Phys. Control. Fusion*. **63**, 094001 (2021). <https://doi.org/10.1088/1361-6587/abffb6>
30. N. Kenmochi, K. Ida, T. Tokuzawa et al., Preceding propagation of turbulence pulses at avalanche events in a magnetically confined plasma. *Sci. Rep.* **12**, 6979 (2022). <https://doi.org/10.1038/s41598-022-10499-z>
31. N. Kenmochi, K. Ida, T. Tokuzawa et al., Fast nondiffusive response of heat and turbulence pulse propagation. *Sci. Rep.* **14**, 13006 (2024). <https://doi.org/10.1038/s41598-024-63788-0>

Publisher's Note Springer Nature remains neutral with regard to jurisdictional claims in published maps and institutional affiliations.